AN IMPROVED BOUNDARY ELEMENT ANALYSIS
OF CAVITATING THREE-DIMENSIONAL HYDROFOILS

Francesco Salvatore & Pier Giorgio Esposito
INSEAN – Italian Ship Model Basin, Rome (Italy)

Abstract

A theoretical analysis of three–dimensional cavitating flows based on a boundary element approach which includes rotational and viscous flow effects is presented. Partial sheet cavitation is studied by a closed–cavity nonlinear model which includes the prediction of the cavity detachment point. The trailing vorticity path is described by a wake–alignment technique. Viscosity effects are included via a viscous/inviscid technique based on boundary–layer assumptions. Cavitation modelling, wake alignment and viscous–flow correction are integrated into the potential–flow solution by BEM through a coupling procedure. Comparisons of present numerical results with experiments and numerical results in the literature show the capability of the proposed methodology to take into account viscosity effects on attached cavitation, and to analyze the flowfield in the tip–vortex region.

1   Introduction

Cavitation on three–dimensional lifting bodies involves extremely complex two–phase flow phenomena whose effects are detrimental for hydrofoils, marine propellers and turbomachinery. Theoretical modelling of those phenomena is still a serious challenge for researchers. Recent developments show the increasing interest for models based on a sophisticated description of the flowfield by using Reynolds Averaged Navier–Stokes (RANS) solvers for single–phase or multi–phase flows (see, *e.g.*, Kato 1996). Those approaches are very promising in that they are capable to describe the interactions between viscosity, vorticity and bubble dynamics. Nevertheless, three–dimensional cavitation analyses are still at an early stage of development and applications are typically limited to two–dimensional flows.

Thus, approaches that are of interest for practical applications are currently based on irrotational–flow assumptions. This imposes severe limitations: *(i)* viscosity effects on sheet cavitation are neglected, *(ii)* the cavity detachment point is poorly predicted, *(iii)* the aft portion of the cavity requires artificial modelling; in addition, simplified descriptions of the trailing vorticity path are used and hence, *(iv)* flowfield analysis is not adequate for tip–vortex cavitation modelling.

The aim of this paper is to present a nonlinear cavitating flow analysis based on a Boundary Element Method (BEM) for potential flows which includes viscous–flow correction and a careful description of the trailing vorticity.

Existing literature on viscous cavitating flow analysis by BEM includes both approaches based on the solution of RANS equations and those based on boundary–layer assumptions. In particular, Chahine & Hsiao (2000) present a coupled RANS/BEM approach in which the attached cavity is determined via an interface tracking method based on BEM, whereas the viscous flow around the body and the cavity is studied by a commercial RANS code. Kinnas, Mishima and Brewer (1994) propose a viscous/inviscid interactive method in which a nonlinear inviscid cavity flow model by BEM is coupled with a boundary–layer analysis around the wetted portion of the body surface and the cavity. Numerical applications are limited to two–dimensional flows. The two approaches above do not include tip–vortex flow analyses. Tip–vortex cavitation by an inviscid–flow BEM is proposed *e.g.*, by Kinnas, Lee and Mueller (1998).

In the present paper, the analysis of three–dimensional cavitation in high–Reynolds number flows by means of a viscous/inviscid coupling technique is proposed. This methodology extends a formulation presented by Esposito & Salvatore (2000) that is limited to two–dimensional flows. The inviscid cavitating flow is studied by a boundary integral formulation for the velocity potential with sheet cavitation modelling. The numerical solution is obtained by a zero–th order BEM. The vortical layer surrounding the body surface, the cavity and the trailing wake is studied by means of a boundary–layer approximation that is valid in the case of attached or slightly separated flows.

Two–dimensional integral boundary–layer equations are solved by using a strip–theory approach. Potential–flow and boundary–layer solutions are matched via an iterative process in which the viscosity correction to the potential flow solution is given in terms of transpiration velocity (Lighthill 1958). The trailing vorticity path is determined by a wake alignment procedure.

Comparisons of present numerical results with experiments on cavitation of three–dimensional hydrofoils are performed in order to assess the capability of the proposed methodology to take into account viscosity effects on sheet cavitation. In particular, the prediction of the cavity detachment point is addressed. In addition, preliminary results on tip–vortex flow analysis are given as a first step towards viscous–flow tip–vortex cavitation modelling.

2 Theoretical analysis of irrotational cavitating flows

Under the assumptions of inviscid and initially irrotational fluid, the perturbation velocity field is irrotational and hence it can be expressed in terms of a scalar potential, ϕ. In a frame of reference fixed to the body, the total velocity field is

$$\mathbf{q} = \mathbf{v}_I + \nabla\phi, \tag{1}$$

where $\mathbf{v}_I$ denotes the unperturbed incoming flow. By incompressible flow assumptions, the potential ϕ satisfies the Laplace equation $\nabla^2\phi = 0$ in the unbounded fluid region $\mathcal{V}_P$ surrounding the body, its trailing wake and the cavity. In the framework of potential flow analyses of lifting bodies, the wake denotes a zero thickness layer where the vorticity generated on the body is shed, and represents a discontinuity surface for ϕ. The cavity denotes the fluid region where vaporization occours: here, partial sheet cavitation is considered, and hence the cavity is assumed to be a thin layer attached to the body surface.

The pressure field in $\mathcal{V}_P$ is given by the Bernoulli equation that, in the frame of reference fixed to the body, reads

$$\frac{\partial\phi}{\partial t} + \frac{1}{2}q^2 + \frac{p}{\rho} + gz_0 = \frac{1}{2}v_I^2 + \frac{p_0}{\rho}, \tag{2}$$

where t denotes time, $q = \|\mathbf{q}\|$, $v_I = \|\mathbf{v}_I\|$, p_0 is the undisturbed–flow pressure, ρ is the fluid density, g is the gravity acceleration and z_0 denotes the depth with respect to the water free surface.

The Laplace equation for ϕ is solved by imposing boundary conditions on $\partial\mathcal{V}_P$. On the portion of the body surface outside the cavity, *i.e.*, on the wetted surface $\mathcal{S}_{WB}$, the impermeability condition yields $\mathbf{q} \cdot \mathbf{n} = 0$, or, recalling Eq. (1) and denoting by $\mathbf{n}$ the outward unit normal to the surface,

$$\frac{\partial\phi}{\partial n} = -\mathbf{v}_I \cdot \mathbf{n} \qquad\qquad \text{on } \mathcal{S}_{WB}. \tag{3}$$

Across the wake surface $\mathcal{S}_W$, pressure and normal component of the perturbation velocity are continuous

$$\Delta p = 0, \qquad\qquad \Delta\left(\frac{\partial\phi}{\partial n}\right) = 0, \qquad\qquad \text{on } \mathcal{S}_W, \tag{4}$$

where Δ denotes discontinuity across the two sides of $\mathcal{S}_W$. By combining the Bernoulli equation (2) and Eqs. (4), one obtains that the potential discontinuity $\Delta\phi$ is convected along wake streamlines, $\Delta\phi(\mathbf{x}_W, t) = \Delta\phi(\mathbf{x}_{WTE}, t - \tau_W)$, where $\mathbf{x}_{WTE}$ is the trailing edge wake point lying on the same streamline as $\mathbf{x}_W$, and τ_W is the convection time from $\mathbf{x}_{WTE}$ to $\mathbf{x}_W$.

A further condition on ϕ is required in order to assure that no finite pressure jump may exist at the body trailing edge (Kutta condition). Following Morino, Chen and Suciu (1975), this is equivalent to impose

$$\Delta\phi(\mathbf{x}_{WTE}, t) = \phi_{TE}^u(t) - \phi_{TE}^l(t), \tag{5}$$

where ϕ_{TE}^u and ϕ_{TE}^l denote, respectively, body trailing edge potentials evaluated on suction and pressure sides.

According to classical sheet cavitation modelling, the cavity is assumed to be a fluid region where the pressure is constant and equal to the vapor pressure p_v, and a non–penetration condition applies on the cavity edge $\mathcal{S}_C$. Thus, by imposing $p = p_v$ on $\mathcal{S}_C$, and by using the Bernoulli theorem (2), yields

$$q = \left[v_I^2\sigma - 2\left(\frac{\partial\phi}{\partial t} + gz_0\right) + v_I^2\right]^{\frac{1}{2}} \qquad\qquad \text{on } \mathcal{S}_C, \tag{6}$$

where $\sigma = (p_0 - p_v)/\frac{1}{2}\rho v_I^2$ denotes the cavitation number. Equation (6) is used to obtain a boundary condition for ϕ on $\mathcal{S}_C$ in terms of σ. By exploiting q in terms of Eq. (1), and by integrating Eq. (6) in chordwise direction, one obtains

$$\phi(s,u) = \phi(s_{CLE}, u) + \int_{s_{CLE}}^{s} \left\{ q_u \cos\theta - v_{I_s} + |\sin\theta| \left[v_I^2\sigma - 2\left(\frac{\partial\phi}{\partial t} + gz_0\right) + v_I^2 - q_u^2 - q_n^2 \right]^{\frac{1}{2}} \right\} d\tilde{s}, \qquad (7)$$

where s, u are curvilinear coordinates on $\mathcal{S}_B$, in chordwise and spanwise directions, respectively; quantities q_s, q_u are the covariant components of $\mathbf{q}$ in the (s, u) coordinate system, $q_n = \mathbf{q} \cdot \mathbf{n}$, and s_{CLE} is the cavity leading edge abscissa.

The condition $p = p_v$ and hence Eq. (7) are not valid in the aft portion of the cavity where pressure tends to wetted–flow conditions through complex two–phase flow phenomena. In the present work, a cavity–closure region is introduced in which pressure is forced to vary smoothly from $p = p_v$ to wetted flow values behind the cavity trailing edge. The fraction λ of the cavity length occupied by the closure region is prescribed (typically, $0.1 < \lambda < 0.3$).

Denoting by $h_c = \mathcal{F}(s, u, t)$ the cavity thickness, and by $\mathcal{S}_{CB}$ the portion of the body surface underneath the cavity, the constant–pressure and the non–penetration conditions on $\mathcal{S}_C$ yield that $\mathcal{S}_C$ is a material surface and hence

$$\frac{\partial\phi}{\partial n} = -\mathbf{v}_I \cdot \mathbf{n} + \chi_c \qquad\qquad \text{on } \mathcal{S}_{CB}, \qquad (8)$$

where $\chi_c = \mathbf{q} \cdot \nabla_s h_c + \partial h_c/\partial t$, and ∇_s denotes the surface gradient on $\mathcal{S}_B$.

3   Viscous flow analysis and coupling

The present viscous–flow analysis is limited to the case of attached high–Reynolds number flows, in which the thickness δ of the vortical layer is assumed to be thin as compared to the thickness of the hydrofoil sections, and hence boundary–layer assumptions are valid. Two–dimensional integral boundary–layer equations are solved by means of a strip–theory approach in which the three–dimensional nature of the flowfield at the boundary–layer edge is taken into account, whereas three–dimensional effects inside the boundary layer are neglected. This limits the application of the proposed approach to the analysis of hydrofoils with moderate skew angle.

In the laminar portion of the boundary layer, the von Kármán equation is solved by using Thwaites' collocation method (Thwaites 1949). The turbulent portion of the boundary layer and the wake are studied by the 'lag–entrainment method' by Green, Weeks and Brooman (1973). Specifically, the von Kármán equation is coupled with two transport equations which model the flow entering the boundary layer (entrainment equation) and the turbulent kinetic energy (lag equation). Michel's method (Michel 1952) is used to predict the transition from laminar to turbulent flow.

The boundary–layer solution is coupled with the potential–flow solution via a viscous/inviscid interactive technique. The boundary–layer equations are solved by using as input the velocity distribution on $\mathcal{S}_{WB} \cup \mathcal{S}_C$ and on the two sides of $\mathcal{S}_W$ obtained by the potential–flow model. Next, the boundary–layer solution determines the viscosity correction to the potential flow. Such correction is given in terms of a transpiration flux across $\mathcal{S}_{WB} \cup \mathcal{S}_C$ and $\mathcal{S}_W$ which, according to Lighthill (1958), takes into account the displacement of the potential flow streamlines due to the presence of the vortical layer. Denoting by $\delta_s^\star$ the displacement thickness of the vortical layer in chordwise direction, the transpiration flux is given by $\chi_v = \partial(q_s^e \delta_s^\star)/\partial s$, where q_s^e is evaluated by the corrected potential–flow model.

Here, the transpiration–flux concept is extended to cavitating flows. Normal–flow conditions over the wetted portion of the body surface, Eq. (3), and across the wake surface $\mathcal{S}_W$, second of Eqs. (4), are modified as follows

$$\frac{\partial\phi}{\partial n} = -\mathbf{v}_I \cdot \mathbf{n} + \chi_v, \qquad \text{on } \mathcal{S}_{WB}; \qquad\qquad \Delta\left(\frac{\partial\phi}{\partial n}\right) = \chi_v{}^u + \chi_v{}^l, \qquad \text{on } \mathcal{S}_W, \qquad (9)$$

where superscripts u and l denote quantities evaluated, respectively, in the wake vortical layers emanating from the suction and pressure sides of the body surface. In addition, Eq. (8), valid on $\mathcal{S}_{CB}$, is formally replaced by

$$\frac{\partial\phi}{\partial n} = -\mathbf{v}_I \cdot \mathbf{n} + \chi_c + \chi_v \qquad \text{on } \mathcal{S}_{CB}. \qquad (10)$$

The boundary–layer and potential–flow solutions are matched through an iterative process.

4   Boundary integral formulation and wake alignment

The potential flowfield including the viscosity correction is determined by means of a boundary integral formulation. By assuming that the perturbation vanishes at infinity, the third Green identity yields

$$E(\mathbf{x},t)\phi(\mathbf{x},t) = \oint_{\mathcal{S}_{WB}\cup\mathcal{S}_C} \left(\frac{\partial\phi}{\partial n}G - \phi\frac{\partial G}{\partial n} \right) d\mathcal{S}(\mathbf{y}) + \int_{\mathcal{S}_W} \left[\Delta\left(\frac{\partial\phi}{\partial n}\right)G - \Delta\phi\frac{\partial G}{\partial n} \right] d\mathcal{S}(\mathbf{y}) \qquad \text{on } \mathcal{V}_P, \quad (11)$$

where $G = -1/4\pi\|\mathbf{x}-\mathbf{y}\|$, whereas E is a domain function equal to $0, 1/2, 1$, respectively, inside, on, or outside $\partial\mathcal{V}_P$.

Equation (11) is solved by using a boundary element approach. The boundary surface and the wake are divided into hyperboloidal quadrilateral elements. Equation (11) in discretized form is evaluated at each centroid of the body surface. Flow quantities are assumed to be constant on each element. The numerical solution of Equation (11) determines ϕ on $\mathcal{S}_{WB}$ and $\partial\phi/\partial n$ on $\mathcal{S}_C$ once $\partial\phi/\partial n$ on $\mathcal{S}_{WB}$, ϕ on $\mathcal{S}_C$, and $\Delta\phi$ on $\mathcal{S}_W$ are given by boundary conditions (5), (7), (9), and by taking into account Eq. (10).

In Eq. (11), both cavity surface $\mathcal{S}_C$ and wake surface $\mathcal{S}_W$ are not known *a priori*. By assuming that the cavity thickness h_c is small as compared to the hydrofoil sections, $\mathcal{S}_C$ in Eq. (11) is replaced by the portion of the body surface underneath the cavity, $\mathcal{S}_{CB}$. This is a usual simplification in three–dimensional cavitation modelling by BEM that avoids additional computational effort required by surface re–panelling and re–calculation of influence coefficients.

The cavity thickness distribution is given by Eq. (8) which, recalling the definition of χ_c, represents a partial differential equation for h_c that may be solved once ϕ and $\partial\phi/\partial t$ are known on $\mathcal{S}_{CB}$. The cavity trailing edge is determined by the condition $h_c = 0$. If this condition is not verified, it is assumed that the guessed planform is too small, and the cavity shape is extrapolated. This procedure is repeated until the cavity planform converges.

The actual shape of $\mathcal{S}_W$ is determined by imposing that wake points move according to the local flow velocity: such procedure is referred to as wake alignment. A boundary integral representation of the perturbation velocity field $\nabla\phi$ is obtained by taking the gradient of both sides of Eq. (11). Once Eq. (11) in dicretized form has been solved, this yields an explicit representation for $\nabla\phi$ at any node $\mathbf{x}_W$ of the discretized wake surface.

Wake alignment is achieved by updating the location of $\mathbf{x}_W$ as follows:

$$\mathbf{x}_W(t+\Delta t) = \mathbf{x}_W(t) + \int_t^{t+\Delta t} \left[\nabla\phi(\mathbf{x}_W,\tau) + \mathbf{v}_I \right] d\tau. \tag{12}$$

In the equation above, time t refers to the convection process of material points along $\mathcal{S}_W$. In discretized form, the left–hand side of Eq. (12) represents the updated location of the wake node lying on the same streamwise strip as $\mathbf{x}_W$ at a distance $\Delta s = q_w\Delta t$, where $q_w = \frac{1}{2}(q^u+q^l)$ is the convection speed. The integral is evaluated by the trapezoidal rule. Starting from an initial guess for $\mathcal{S}_W$, Eq. (12) is used to update the location of each wake node. Once $\mathcal{S}_W$ has been modified, the potential field is re–computed by Eq. (11). The process is repeated until convergence of the wake shape.

The evaluation of the influence coefficients in the boundary integral equations above is performed by using analytical integration as proposed by Morino *et. al.* (1975). In addition, the contribution to $\nabla\phi$ given by doublets $\partial G/\partial n$ distributed on $\mathcal{S}_W$ is calculated by using the equivalence between the velocity induced by a constant doublet distribution on a quadrilateral panel and that induced by a square vortex ring lying on the panel edges (Campbell 1973). If the distance r from the vortex is less than a given value r_δ, the intensity of the velocity induced by the vortex is evaluated as a linear function of r. This corresponds to introduce a rough modelling of the velocity defect into the viscous vortical layer surrounding the wake surface $\mathcal{S}_W$, and prevents from numerical instabilities. In the present approach, the vortex core radius r_δ equals the vortical–layer thickness in the wake predicted by the boundary–layer solution.

5   Solution procedure

A crucial issue related to the present BEM is the procedure chosen to include simultaneously nonlinear effects related to viscous–flow correction, wake alignment and cavitation modelling. The proposed procedure is based on the assumption that the flowfield perturbation induced by the cavity has a negligible impact on the location of the wake surface (see Sec. 6). Thus, the wake alignment procedure is performed under non–cavitating flow conditions. Once the actual shape of the trailing wake has been determined, an initial guess for the cavity trailing edge is imposed and the cavitation model is switched on. The non–cavitating wake–alignment stage is coupled with a boundary–layer solution in order to obtain: *(i)* the vortex core thickness r_δ to be used in the wake–alignment procedure, as described in Sec. 4, and *(ii)* a guess for the location of the cavity detachment line, as discussed below in Sec. 6.

Once the cavitation model is switched on, viscous/inviscid coupling is performed. The cavitating–flow analysis is repeated until convergence of the cavity shape and hence the solution of the boundary–layer equations is updated. This procedure is repeated until $\Delta \mathcal{V}_C \leq 1 \times 10^{-3}$ and $\Delta \mathcal{D}_v \leq 1 \times 10^{-3}$, where $\Delta \mathcal{V}_C$ and $\Delta \mathcal{D}_v$ denote, respectively, difference between cavity volume and viscous drag computed at two successive iterations. Typically, $4 \div 5$ iterations are required to converge. Within each iteration, the evaluation of the cavity shape converges in $2 \div 10$ steps.

6 Numerical results

Validation of three–dimensional cavitating flow predictions has been performed by considering an experiment performed at the MIT Marine Hydrodynamics Tunnel. Details of the hydrofoil geometry and test conditions are given by Kinnas & Fine (1993). The hydrofoil, a windsurfer fin, has a rounded tip, span $D = 2.63c$, where c is the root chord. Cavity planform measurements at $\sigma = 1.084$ and $\sigma = 1.148$, Reynolds number $Re = 9 \times 10^5$, and angle of attack $\alpha = 6.5°$ are reported by Kinnas & Fine (1993).

First, the influence of the body surface discretization on numerical results has been examinated: N_s and N_u denote, respectively, the number of discretization elements along hydrofoil chord and span. A sensitivity analysis (not reported here) shows that using $N_u > 20$ does not modify cavity planform predictions significantly. The influence of the parameter N_s is shown in Figs. 1 and 2. Figure 1 depicts cavity volumes at $\sigma = 1.148$ obtained by varying N_s with fixed $N_u = 20$, whereas Fig. 2 shows the corresponding cavity thickness distributions at a representative chordwise section. It may be concluded that, if $N_s \geq 50$, discretization errors are negligible. Hence, numerical results described below have been obtained by using $N_s = 60$, $N_u = 20$. In addition, the wake surface has been discretized by using $N_w = 30$ elements in the streamwise direction and N_u elements in the transverse direction.
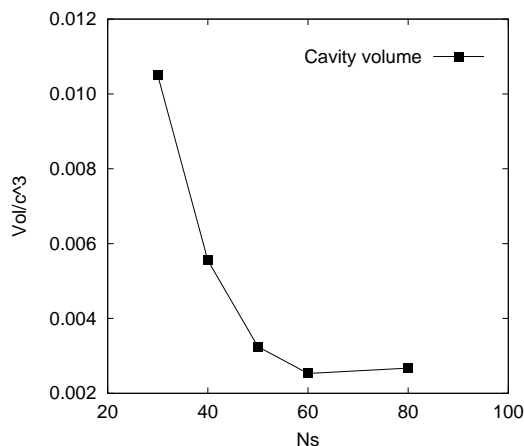
Figure 1: Effect of grid parameter N_s on cavity volume: fin, $\sigma = 1.148$.
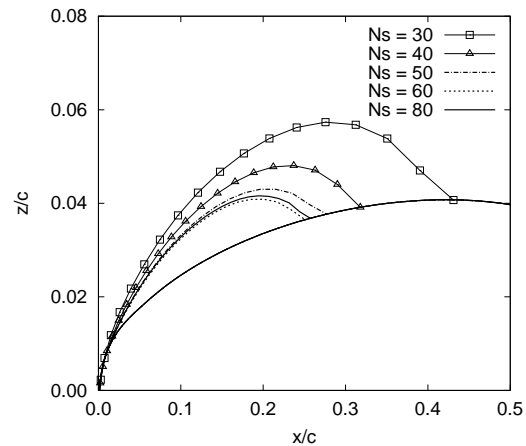
Figure 2: Effect of grid parameter N_s on cavity thickness: fin chordwise section at $y/D = 0.6$, $\sigma = 1.148$.

One of the major problems of cavitation modelling by inviscid–flow methods is the localization of the cavity detachment point, x_d. Computed cavity patterns strongly depend on this quantity, and hence predictions may be unreliable. This is illustrated by Fig. 3 which depicts cavity planforms obtained by forcing x_d to different values. In the present approach, cavity detachment is imposed where a sharp increase of the shape factor H–ratio between displacement thickness and momentum thickness–is determined by solving the laminar boundary–layer. As an example, Fig. 4 depicts the chordwise distribution of H in the leading–edge region at various steps of the viscous/inviscid coupling (VIC) procedure: $H = 3$ is used to determine x_d. The first–step solution is obtained under wetted–flow conditions, whereas cavitation modelling is included from the second step. It may be observed that the cavity detachment location predicted under wetted–flow conditions is a good approximation of the converged result (step 4).

Cavity extension predictions by using the viscous/inviscid coupling are given in Fig. 5 ($\sigma = 1.084$) and in Fig. 6 ($\sigma = 1.148$). Present results are compared to measurements by Kinnas & Fine (1993), and to numerical results by Pelleat & Pellone (1996), obtained by an inviscid–flow model in which the location of the cavity detachment line is
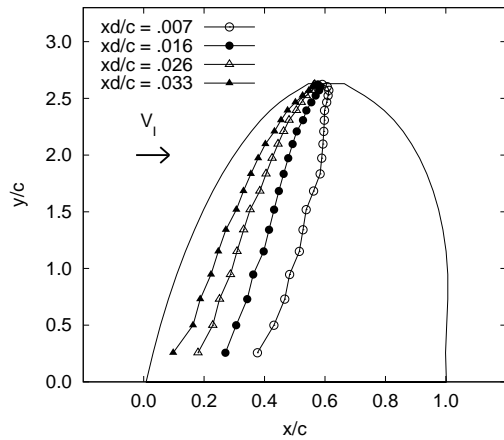
Figure 3: Effect of parameter x_d on cavity planform: fin, $\sigma = 1.148$.
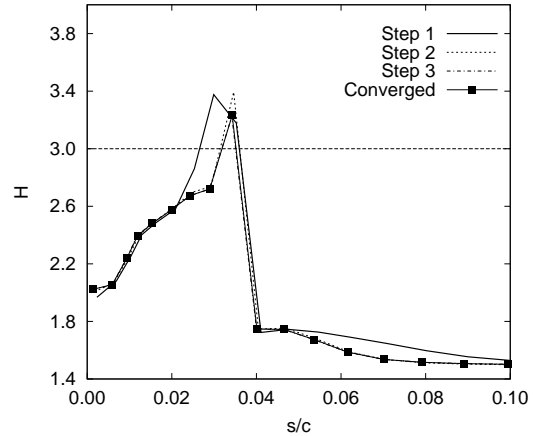
Figure 4: Shape factor distribution at different steps of VIC: fin chordwise section $y/D = 0.05$, $\sigma = 1.148$.
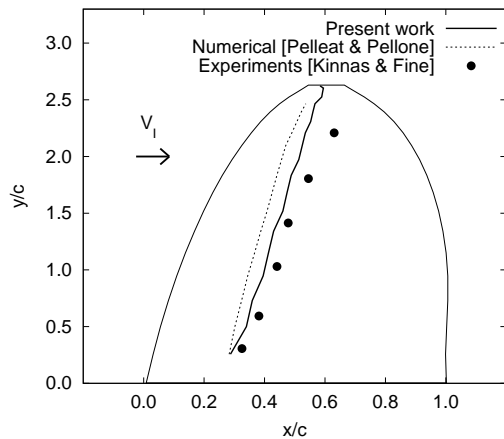
Figure 5: Cavity planform prediction: fin, $\sigma = 1.084$.
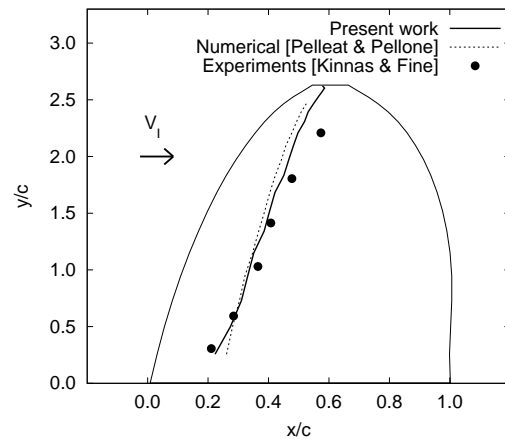
Figure 6: Cavity planform prediction: fin, $\sigma = 1.148$.

prescribed. Both numerical results are in satisfactory agreement with experiments with the only exception of the tip region. It should be observed that measurements report $x_d/c = 0.024$ constant along the span for both σ values, present results predict $0.02 < x_d/c < 0.035$, whereas $x_d/c = 0.006$ is used by Pelleat & Pellone (1996).

It is worthwhile to evaluate the viscosity effects on cavitation if the cavity detachment point is prescribed. Figure 7 shows cavities obtained by using the viscous/inviscid coupling (VIC) technique and by using the invisicid–flow model. In both calculations, x_d has been forced to a fixed value. It is apparent that viscosity tends to reduce both cavity extension and thickness. (In Fig. 7 and in Fig. 8 below, the cavity thickness is multiplied by a factor 5).

The calculations above do not include wake alignment. In particular, a prescribed wake having a cylindrical shape aligned to the unperturbed flow has been used. Hence, it is necessary to evaluate the influence of wake alignment on cavitating flow predictions. One of the conclusions of the present study is that the shape of the wake has a negligible influence on attached cavities whose chordwise extension at the tip does not exceed $50 \div 60\%$ of hydrofoil chord. In such cases, cavities obtained by combining viscous/inviscid coupling and wake alignment are identical within plotting accuracy to those obtained by using viscous/inviscid coupling with a prescribed cylindrical wake (result not shown here). Figure 8 illustrates a result obtained by combining viscous/inviscid coupling and wake alignment. Computed cavity profiles at some sections along the span are shown. It is apparent the roll–up of the wake tip. The flowfield in the tip region is strongly influenced by the thickness r_δ of the vortex core. The smoothness of the wake shape in that region demonstrates that reliable values for r_δ are predicted by the present boundary–layer solution.
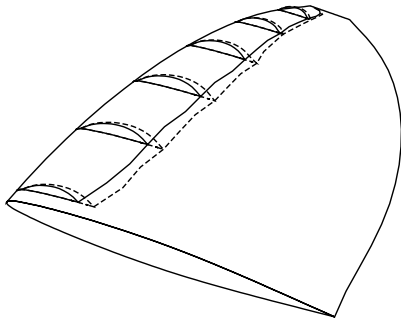
Figure 7: Viscosity effects on cavity planform. Solid line: VIC; dashed line: Potential flow. Fin, $\sigma = 1.148$.
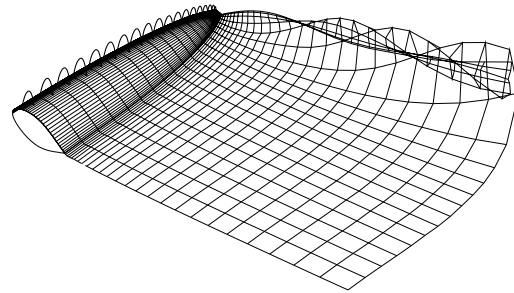
Figure 8: Predicted attached cavity and trailing wake: Fin, $\sigma = 1.148$, $Re = 1 \times 10^6$.
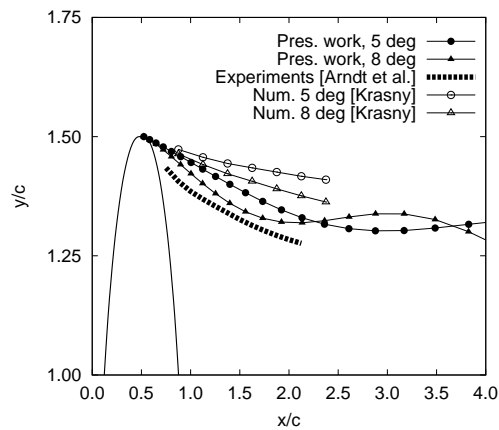
Figure 9: Tip–vortex location: non–cavitating flow, elliptic wing ($Re = 1 \times 10^6$ in present results).
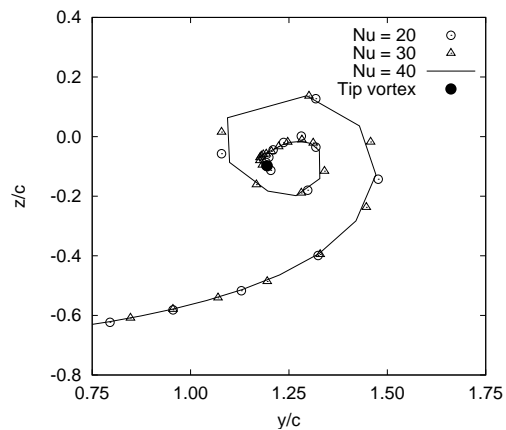
Figure 10: Tip–vortex shape at $x/c = 8.0$. Non–cavitating flow, $\alpha = 5°$, elliptic wing.

The importance of wake alignment combined to cavitation modelling is related to the analysis of tip–vortex flow. In particular, accurate predictions of the tip–vortex location may be obtained. In order to demonstrate this, experimental observations of tip–vortex cavitation of an elliptical hydrofoil by Arndt, Arakeri and Higuchi (1991) have been considered. The hydrofoil has an elliptic planform and aspect ratio $A = 3$ (see Arndt *et al.* 1991, for details). Figure 9 depicts the tip–vortex trajectories measured in several tests with $Re = 5.3 \times 10^5 \div 1.04 \times 10^6$, $\alpha = 3° \div 13°$, and $\sigma = 0.26 \div 3.19$. Experiments are compared to present calculations by using the non–cavitating viscous/inviscid approach with wake alignment and to numerical results obtained by Krasny (1987) by using a two–dimensional vortex sheet model for non–cavitating flows. In spite of the wide range of variations for both α, Re and σ, the measured trajectories present a small spread, as represented by the thickness of the dashed curve in Fig. 9. In particular, Arndt *et al.* (1991) observe that the tip–vortex location is slightly influenced by the hydrofoil loading and hence by the occurrence of cavitation. This is confirmed in part by present calculations which determine helical tip–vortex paths with helicoid axes at $\alpha = 5°$ and $\alpha = 8°$ that are close each other. On the contrary, a strong dependence of the tip–vortex path by α is found by Krasny (1987) which uses a two–dimensional model that does not take into account the strong three–dimensional nature of the roll–up process at the wake tip, as shown by Fig. 8.

Finally, Fig. 10 shows the computed wake surface under non–cavitating flow conditions with $\alpha = 5°$ and $Re = 1 \times 10^6$. A detail of the wake tip–vortex region in a vertical plane at a distance $x/c = 8$ from the hydrofoil root trailing edge is presented. The location of the numerical tip–vortex, *i.e.*, of the wake streamline emanating from the hydrofoil tip, is also shown. It is apparent that $N_u = 20$ discretization elements in spanwise direction are sufficient to have a careful description of the roll–up process.

7   Conclusions

A theoretical analysis of cavitation on three–dimensional hydrofoils has been presented. The proposed methodology is based on a boundary element method in which cavitation modelling, wake alignment and viscous–flow correction are integrated into the potential–flow solution by a coupling procedure. The boundary layer solution allows to predict cavity detachment, and hence one of the major drawback of inviscid–flow cavitation models is overcome. In addition, wake alignment allows to evaluate the tip–vortex trajectory and hence to localize tip–vortex cavitation. The thickness of the tip–vortex core is related to the thickness of the boundary layer at the body trailing edge.

Numerical results show the capability of the proposed approach to give accurate predictions of attached cavitation. The influence of viscosity on cavity thickness and extension is discussed. The localization of the tip–vortex is satisfactory as compared to experimental measurements. A detailed investigation (only in part reported here due to lack of space) has been conducted in order to determine the discretization requirements that are necessary to obtain reliable predictions in terms of cavitation, boundary–layer solution and wake alignment procedure. This is of primary importance in view of the extension of the present approach to the analysis of cavitation of marine propellers.

Further refinements of the present approach should be obtained by including the solution of fully three–dimensional boundary–layer equations and tip–vortex cavitation modelling.

Acknowledgments

References

Arndt, R.E.A., Arakeri, V.H. and Higuchi, H. (1991). Some observations of tip–vortex cavitation. *J. Fluid Mech.,* **229**, 269–289.

Campbell, (1973). *Foundations of fluid flow theory*. Addison–Wesley.

Chahine, G.L. & Hsiao, C.T. (2000). Modelling 3D unsteady sheet cavities using a coupled UnRANS–BEM code. In *Proc. 23rd ONR Symposium on Naval Hydrodynamics*.

Esposito, P.G. & Salvatore, F. (2000). Optimal design of cavitating blade sections by genetic algorithms. In *Proc. NCT '50 Int. Conf. on Propeller Cavitation*, 446–465.

Green, J.E., Weeks, D.J., and Brooman, W.F. (1973). Prediction of turbulent boundary layers and wakes in compressible flow by a lag–entrainment method. *A.R.C.R. & M. Tech. Rep.* 3791.

Kato, H. (1996). *Cavitation*. In *Advances in Marine Hydrodynamics – Chapter V*. Ed. by M. Ohkusu. Computational Mechanics Publications.

Kinnas, S.A. & Fine, N. (1993). A numerical nonlinear analysis of the flow around two– and three–dimensional partially cavitating hydrofoils. *J. Fluid Mech.,* **254**, 151–181.

Kinnas, S.A., Mishima, S. and Brewer, W. (1994). Nonlinear analysis of viscous flow around cavitating hydrofoils. In *Proc. 20th ONR Symposium on Naval Hydrodynamics*, 446–465.

Kinnas, S.A., Lee, H. and Mueller, A. (1998). Prediction of propeller blade sheet and developed tip vortex cavitation.. In *Proc. 22nd ONR Symposium on Naval Hydrodynamics*, 182–198.

Krasny, R. (1987). Computation of vortex sheet roll–up in the Trefftz plane. *J. Fluid Mech.,* **184**, 123–155.

Lighthill, M.J. (1958). On displacement thickness. *J. Fluid Mech.,* **4**, 383–392.

Michel, R. (1952). Etude de la transition sur les profils d'aile - establissment d'un point de transition et calcul de la trainée de profil en incompressible. *ONERA Tech. Rep.* 1/1578A.

Morino, L, Chen, L.T. and Suciu, E. (1975). Steady and oscillatory subsonic and supersonic aerodynamics around complex configurations. *AIAA J.*, **13**, 368–374.

Pelleat, J.M. & Pellone C. (1996). Experimental validation of two– and three–dimensional numerical analysis of partially cavitating hydrofoils. *J. Ship Res.,* **40**, 211–223.

Thwaites, B. (1949). Approximate calculation of the laminar boundary layer. *Aeronaut. Quart.,* **1**, 245–280.